

# Power loss minimization assessment of a doubly fed induction generator with variable core resistance for wind turbines operation

Crescent Onyebuchi Omeje<sup>1</sup>, Damian Benneth Nnadi<sup>2</sup>

<sup>1</sup>Department of Electrical/Electronic Engineering, University of Port Harcourt, Choba, Port Harcourt, Rivers State, Nigeria

<sup>2</sup>Department of Electrical Engineering, University of Nigeria, Nsukka Enugu State, Nigeria

## Article Info

### Article history:

Received Oct 1, 2022

Revised Oct 30, 2022

Accepted Nov 7, 2022

### Keywords:

Doubly fed induction generator

Hessian matrix

Power loss modeling

Simulations

Transient stability

## ABSTRACT

This paper assesses the efficiency level and power loss minimization of a doubly fed induction generator (DFIG). A modified DFIG equivalent circuit with multi-core resistance connected in parallel was adopted. State-space differential equations of the DFIG was developed incorporating iron and copper loss components while a minimum flux linkage that aids in the minimization of the overall losses was derived. Simulation results showed that losses were minimized when the equivalent core resistances were connected in parallel with minimum permissible current flow. The results obtained during a transient disturbance showed that at different core resistance values of  $R_{fe} = 0.75\Omega$  and  $0.25\Omega$ , different efficiency values of 83.45% and 41.21% were realized. An unconstrained optimization test carried out on the DFIG variable parameters showed that the DFIG power loss model was controllable with a positive definite value of 691.9801 and 2.9156 [e] <sup>^(+5)</sup> for the leading principal determinants of the Hessian matrix. All simulation processes were achieved in MATLAB/Simulink 2020.

This is an open access article under the [CC BY-SA](#) license.



## Corresponding Author:

Crescent Onyebuchi Omeje

Department of Electrical/Electronic Engineering, University of Port Harcourt

East-West Road, PMB, 5323 Choba, Port Harcourt Rivers State, Nigeria

Email: crescent.omeje@uniport.edu.ng

## 1. INTRODUCTION

Wind energy in addition to photovoltaic energy source is the fastest growing energy with an annual growth rate of 30% and with a predictable penetration of 12% of the global electricity demand [1]. The use of power electronic converters allows for a variable speed operation of the wind turbine where the wind energy conversion system extracts maximum power from the turbine during peak operation as reported in [2]. One of the energy generation systems commercially available in the wind energy market is the doubly fed induction generator (DFIG) and its numerous advantages are enumerated in [2], [3]. To produce a maximum energy, an efficient DFIG with higher power rating is a precondition for wind energy conversion system (WECS) though active power loss during the operation is the main drawback for efficiency optimization and life expectancy's challenge. Variable speed wind turbines are usually more effective due to their improved efficiency in capturing more wind power and their innate ability to achieve higher quality of power at optimum wind speed [4]. DFIG implementation is increasing in leaps and bounds as a consequence of a reduced mechanical stress and noise in addition to the flexible control of active and reactive power which is based on the back-to-back power electronics converter sandwiched between the induction machine and the power grid [5]. Active power generation at the stator and rotor terminals is effectively controlled using the rotor side converter (RSC). The regulation of the stator side active and reactive power is independently

achieved with the RSC. However, the fluctuations in power output from the DFIG-based wind generation in response to the variations in wind speed adversely affect the needed power quality [6]. Therefore, with an increased penetration of the DFIG in power system operation, inertia of the power system is reduced. An increased capacity in grid integration of this variable power poses an impactful challenge on power system stability [7]. In line with the system stability is the minimization of the overall system losses under different wind speed and reactive power conditions. Therefore, to improve on the system overall efficiency, the reactive power flow is regulated with a minimized system electrical loss on the generator and on the power electronic converters.

In this paper, a modified equivalent circuit of the DFIG with variable core resistance values for loss minimization was adopted. The copper and iron losses of the DFIG were modeled as a function of the rotor dq-axes currents and stator flux. At optimum condition, the stator d-axis flux that minimizes the total DFIG loss was derived. The simulation results obtained showed that the efficiency values of 83.45% and 41.21% were obtained when the equivalent paralleled core resistance values of the DFIG were kept at  $0.75\Omega$  and  $0.25\Omega$ . The power loss at a slight transient disturbance peaked at 202.277 kW and reduced to 17.2058 kW under steady state for  $0.75\Omega$  net resistance. Similarly, at a net core resistance value of  $0.25\Omega$ , the power loss during a transient disturbance peaked at 757.325 kW and reduced to 23.7597 kW. The variations in the power loss at different net-core resistance accounted for the difference in the efficiency values as presented in the preceding simulation waveforms.

This paper is organized as follows: Section 1 is the introduction; Section 2 is the reviewed literature on DFIG loss control; Section 3 illustrates the wind turbine model of doubly fed induction generator; Section 4 presents the DFIG mathematical modeling and power loss minimization scheme; and Section 5 contains the simulation results. Section 6 is the conclusion.

## 2. METHODOLOGY AND REVIEWED LITERATURE ON DFIG POWER LOSS CONTROL

Research procedures and methods applied in this paper involved mathematical modeling of the doubly fed induction generator at variable core resistances to determine its effects on the overall power loss of the system. Stability test using the Sylvester criterion method and data acquisition derived from simulation parameters were parts of the methods applied in the empirical analysis of the system controllability. In [8]–[10], direct power control (DPC) and direct torque control of the DFIG was proposed as a conventional control scheme. However, large torque and power ripples are the two major draw backs associated with this method. The various methods involving back stepping direct power control strategy for DFIG have been presented in [11]–[14]. Although a detailed analysis was presented but emphasis on variable core resistance and minimum flux at which the DFIG power loss is minimized was not presented.

In [15], [16], a sliding mode approach in minimizing copper loss was presented in a nonlinear control application while a coordinated predictive control of the DFIG using non-Gaussian wind power predictive distribution was reported in [17]. The reports concentrated on regulating the extracted power from the wind turbine while incorporating machine loss minimization technique for iron-loss. In [18], [19], minimization of the active and reactive power ripples using the direct power control of matrix converter fed DFIG was presented without reference to the DFIG core losses minimization.

This paper therefore analyzed a complete loss minimization of the DFIG using the parameter variation that involves the core resistance and stator flux. A complete DFIG loss equation was modeled and derived from a modified equivalent circuit involving the variable core resistance while a minimal flux equation that minimized the DFIG losses was also derived. The Sylvester criterion using the Hessian matrix was applied to determine if the DFIG total power loss was minimized within the context of the variable core resistance values chosen. Therefore, with the leading principal determinants positive for  $R_{eq} = R_{fe} = 0.25\Omega$  and  $0.75\Omega$ , it showed that the overall total loss of the DFIG is controllable and so is minimized.

## 3. WIND TURBINE MODEL OF DOUBLY FED INDUCTION GENERATOR.

The schematic diagram of the DFIG wind turbines operation is presented in Figure 1. The DFIG stator is directly connected to the grid through the grid side converter GSC and its rotor terminal is connected to the rotor side converter RSC through the slip rings. The wind turbine is modeled with reference to optimal power tracking to provide a maximum energy capture from the wind. The aerodynamic model of the wind turbine gives a coupling between the wind speed and the mechanical torque produced by the wind turbine. Aerodynamic is a science of physical laws that deals with the behavior of objects in airflow and forces that are produced by this airflow. The aerodynamic power equation extracted from the wind turbines is given by (1) as reported in [20]–[22].

$$P_m = \frac{1}{2} \times \rho \times A \times V^3 \times C_p \times (\lambda, \beta) \quad (1)$$

Where  $P_m$  (W) is the mechanical power of the turbine,  $\rho$  (Kg/m<sup>3</sup>) is the air density,  $A$  (m<sup>2</sup>) is the area covered by the rotor turbine,  $V$  (m/s) is the wind speed upstream of the rotor and  $C_p$  is the performance coefficient or power coefficient. The power coefficient is a function of the pitch angle ( $\beta$ ) of the rotor blades. The tip speed ratio is the ratio between the blade tip speed and wind speed upstream of the rotor. Altering the pitch angle implies slightly rotating the turbine blades along the horizontal or vertical axis.  $C_p$  which represents the wind turbine power coefficient is given by (2).

$$C_p(\lambda, \beta) = 22 \times \left( \frac{1.16}{\lambda_i} - 0.004\beta - 0.05 \right) e^{-\frac{12.5}{\lambda_i}} \quad (2)$$

$$\frac{1}{\lambda_i} = \frac{1}{\lambda + 0.08\beta} - \frac{0.035}{\beta^3 + 1} \quad (3)$$

Where  $\beta$  represents the blade pitch angle and  $\lambda$  represents the tip speed ratio which is given by (4).

$$\lambda = \frac{\omega_r R_r}{V} \quad (4)$$

The dynamic model wind turbine is associated with the rotor speed  $\omega_r$  and gear box ratio  $\eta_g$  by (5).

$$\omega_r = \eta_g \times \omega_r^{optimum} \quad (5)$$

The exact dynamic model of the torque equation for the generator is given by (6).

$$T_m = \frac{P_m}{\omega_r} = \frac{\pi \rho R^3}{2} \times V_w^2 \times C_t(\lambda) \quad (6)$$

Where  $\rho$  = air density (Kg m<sup>-3</sup>);  $R$  = radius of the turbine (m);  $V_w$  = wind speed (MS<sup>-1</sup>);  $C_t(\lambda)$  = Torque coefficient (pu). The wind turbine characteristics are presented in Figure 2.

The plot of power coefficient against the tip speed ratio at varying blade pitch angle is represented in Figure 2. It is observed that the power coefficient increases as the pitch angle decreases. Therefore, at a zero-pitch angle, the maximum power coefficient is 0.5 which implies that the maximum power is tracked at a zero-blade pitch and tip speed ratio value of ten as shown in Figure 2.

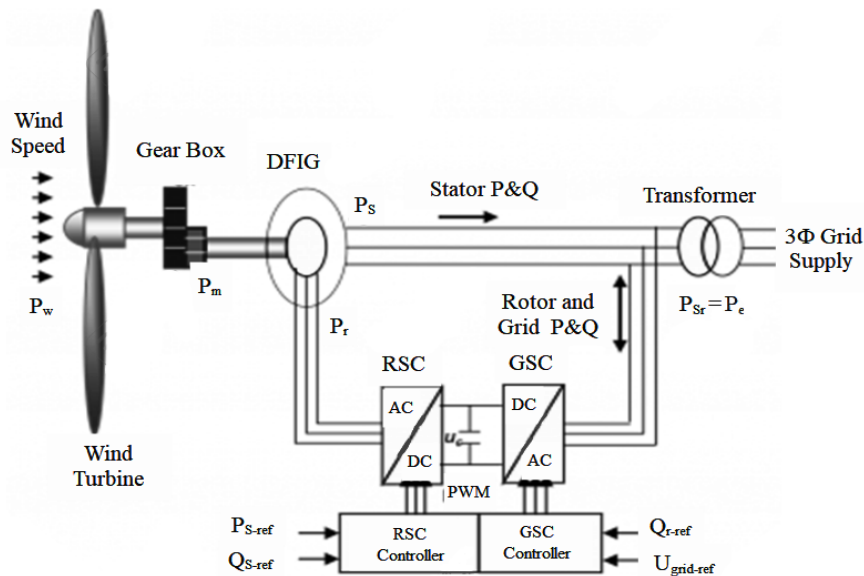


Figure 1. Schematic diagram of a DFIG operated wind turbine

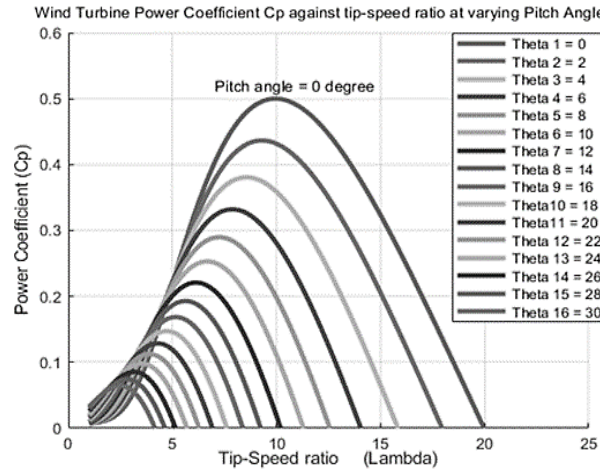


Figure 2. A plot of wind turbine power coefficient against tip-speed ratio at varying pitch angle

#### 4. DFIG MATHEMATICAL MODELING AND POWER LOSS MINIMIZATION SCHEME.

Stator and rotor voltage as well as flux equations as reported in [23], [24] are given in (7)–(14)

$$V_{ds} = R_s i_{ds} + \frac{d\lambda_{ds}}{dt} - \omega_e \lambda_{qs} \quad (7)$$

$$V_{qs} = R_s i_{qs} + \frac{d\lambda_{qs}}{dt} + \omega_e \lambda_{ds} \quad (8)$$

$$V_{dr} = R_r i_{dr} + \frac{d\lambda_{dr}}{dt} - \omega_e \lambda_{qr} \quad (9)$$

$$V_{qr} = R_r i_{qr} + \frac{d\lambda_{qr}}{dt} + \omega_e \lambda_{dr} \quad (10)$$

$$\lambda_{ds} = L_{Ls} i_{ds} + L_m i_{dm} \quad (11)$$

$$\lambda_{qs} = L_{Ls} i_{qs} + L_m i_{qm} \quad (12)$$

$$\lambda_{dr} = L_{Lr} i_{dr} + L_m i_{dm} \quad (13)$$

$$\lambda_{qr} = L_{Lr} i_{qr} + L_m i_{qm} \quad (14)$$

Modified voltage equations can be obtained by substituting (11)–(14) into (7)–(10).

$$V_{ds} = R_s i_{ds} + L_{Ls} \frac{di_{ds}}{dt} + L_m \frac{di_{dm}}{dt} - \omega_e (L_{Ls} i_{qs} + L_m i_{qm}) \quad (15)$$

$$V_{qs} = R_s i_{qs} + L_{Ls} \frac{di_{qs}}{dt} + L_m \frac{di_{qm}}{dt} + \omega_e (L_{Ls} i_{ds} + L_m i_{dm}) \quad (16)$$

$$V_{dr} = R_r i_{dr} + L_{Lr} \frac{di_{dr}}{dt} + L_m \frac{di_{dm}}{dt} - \omega_e (L_{Lr} i_{qr} + L_m i_{qm}) \quad (17)$$

$$V_{qr} = R_r i_{qr} + L_{Lr} \frac{di_{qr}}{dt} + L_m \frac{di_{qm}}{dt} + \omega_e (L_{Lr} i_{dr} + L_m i_{dm}) \quad (18)$$

Modified equivalent circuit model of the DFIG with multiple paralleled core resistance is obtained from (15)–(18) and presented in Figures 3 and 4. Branch currents are obtained from Figures 3 and 4 by applying KCL as expressed in (19) and (20).

$$i_{ds} + i_{dr} = i_{dm} + \frac{[-\omega_e L_m i_{qm}]}{R_{eq}} = i_{dm} - A i_{qm} \quad (19)$$

$$i_{qs} + i_{qr} = i_{qm} + \frac{[\omega_e L_m i_{dm}]}{R_{eq}} = i_{qm} + A i_{dm} \quad (20)$$

A simultaneous solution of (19) and (20) by substitution gives rise to (21) and (22).

$$i_{dm} = \frac{[(i_{ds} + i_{dr}) + A(i_{qs} + i_{qr})]}{(1 + A^2)} \quad (21)$$

$$i_{qm} = \frac{[(i_{qs} + i_{qr}) + A(i_{ds} + i_{dr})]}{(1 + A^2)} \quad (22)$$

Where:  $A = \frac{\omega_e L_m}{R_{eq}}$ . For vector controlled condition,  $\lambda_{qs} = 0$  and  $\lambda_{ds} = \lambda_s$  substituting this into (11) and (12) gives rise to (23) and (24).

$$i_{qs} = \frac{-L_m}{L_{Ls}} i_{qr} \quad (23)$$

$$i_{ds} = \frac{\lambda_s - L_m i_{dr}}{L_{Ls}} \quad (24)$$

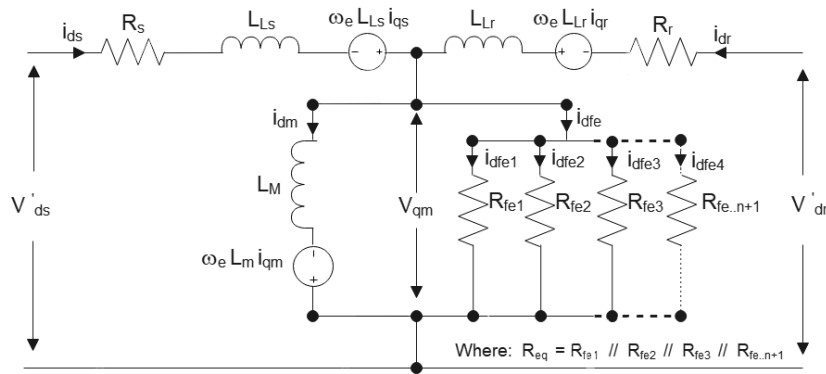


Figure 3. D-axis equivalent circuit of a DFIG with multiple paralleled core resistance

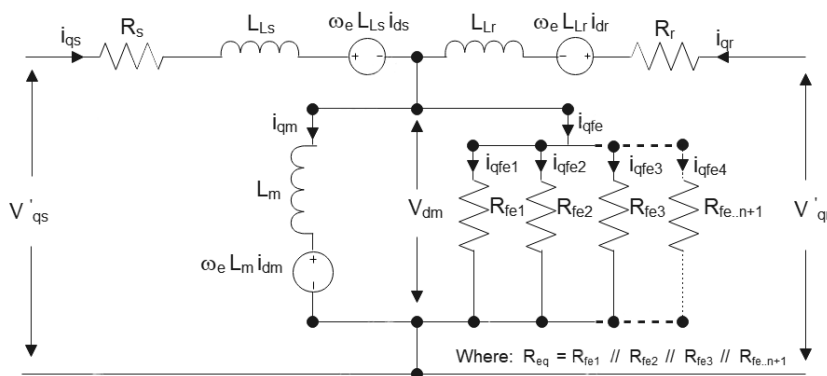


Figure 4. Q-axis equivalent circuit of a DFIG with multiple paralleled core resistance

Therefore, the dq-axes magnetizing currents under vector control is obtained by substituting (23) and (24) into (21) and (22) as re-presented in (25) and (26).

$$i_{dm} = \frac{[\lambda_s + (L_{Ls} - L_m)(i_{dr} + A i_{qr})]}{L_{Ls}(1 + A^2)} \quad (25)$$

$$i_{qm} = \frac{[(L_{Ls}-L_m)(i_{qr}-A_{idr})-A\lambda_s]}{L_{Ls}(1+A^2)} \quad (26)$$

The dq-axes magnetizing voltages are presented in (27) and (28).

$$V_{dm} = -\omega_e L_m i_{qm} = \frac{A\omega_e L_m \lambda_s}{L_{Ls}(1+A^2)} + \frac{\omega_e L_m L_{Ls}(A_{idr}-i_{qr})}{L_{Ls}(1+A^2)} = A_1 A \lambda_s + A_2 (A_{idr} - i_{qr}) \quad (27)$$

$$V_{qm} = -\omega_e L_m i_{dm} = \frac{\omega_e L_m \lambda_s}{L_{Ls}(1+A^2)} + \frac{\omega_e L_m L_{Ls}(i_{dr} + A_{iqr})}{L_{Ls}(1+A^2)} = A_1 \lambda_s + A_2 (i_{dr} + A_{iqr}) \quad (28)$$

Where:  $A_1 = \frac{\omega_e L_m}{L_{Ls}(1+A^2)}$  and  $A_2 = L_{Ls} A_1$ .

The voltage magnitude across the magnetizing branch is presented in (29).

$$V_m^2 = V_{dm}^2 + V_{qm}^2 = A_2^2(1+A^2)[i_{dr}^2 + i_{qr}^2] + 2A_1 A_2(1+A^2)\lambda_s i_{dr} + A_1^2(1+A^2)\lambda_s^2 \quad (29)$$

Total core loss in terms of magnetizing voltage and equivalent core resistance is given by (30).

$$P_{core}^{Total} = \frac{(V_m)^2}{R_{eq}} = \frac{1}{R_{eq}} A_2^2(1+A^2)(i_{dr}^2) + 2A_1 A_2(1+A^2)\lambda_s i_{dr} + A_1^2(1+A^2)\lambda_s^2 \quad (30)$$

Where:  $i_r^2 = i_{dr}^2 + i_{qr}^2$  and  $R_{eq} = R_{fe} \| R_{fe} \| R_{fe} \dots n+1$  are derived from Figures 3 and 4. The stator and rotor copper losses with core losses which are the total resistive losses of the DFIG are presented in (31).

$$P_{Resistive}^{Total} = R_s[i_{ds}^2 + i_{qs}^2] + R_r[i_{dr}^2 + i_{qr}^2] + R_{fe}[i_{qfe}^2 + i_{dfe}^2] \quad (31)$$

Substituting (23) and (24) into (31) gives rise to (32).

$$P_{Resistive}^{Total} = \frac{R_s(\lambda_s)^2}{L_{Ls}^2} + \frac{R_s L_m^2}{L_{Ls}^2} (i_{dr})^2 - \frac{2R_s L_m}{L_{Ls}^2} \lambda_s i_{dr} + \frac{R_s L_m^2}{L_{Ls}^2} (i_{qr})^2 + R_r i_r^2 + R_{fe}[i_{qfe}^2 + i_{dfe}^2] \quad (32)$$

Other types of power losses associated with the DFIG operated system are the RL-filter losses, Frictional losses and power electronics converter losses as presented in (33)–(35) respectively.

$$P_{RL-Filter} = R_{Filter}(i_{d-Filter}^2 + i_{q-Filter}^2) \quad (33)$$

$$P_{Friction} = K_{Fr} \omega_{mech}^2 \quad (34)$$

$$P_{Converter} = R_{Converter}(i_{d-Converter}^2 + i_{q-Converter}^2) \quad (35)$$

The total losses of the DFIG scheme can be written in terms of the total core loss, resistive loss, RL-filter losses, Frictional losses and power electronics converter losses as given in (36).

$$P_{Loss}^{Total} = P_{core}^{Total} + P_{Resistive}^{Total} + P_{RL-Filter} + P_{Friction} + P_{Converter} = \frac{1}{R_{eq}} [A_2^2(1+A^2)i_{dr}^2 + 2A_1 A_2 \lambda_s i_{dr}(1+A^2) + A_1^2 \lambda_s^2(1+A^2)] + \frac{R_s(\lambda_s)^2}{L_{Ls}^2} + \frac{R_s L_m^2}{L_{Ls}^2} i_{dr}^2 - \frac{2R_s L_m}{L_{Ls}^2} \lambda_s i_{dr} + R_r i_r^2 + R_{fe}[i_{qfe}^2 + i_{dfe}^2] + R_{Filter}(i_{d-Filter}^2 + i_{q-Filter}^2) + K_{Fr} \omega_{mech}^2 + R_{Converter}(i_{d-Converter}^2 + i_{q-Converter}^2) \quad (36)$$

The flux at which Total Power loss is minimized is determined by setting the derivative of (36) to zero.

$$\frac{dP_{Loss}^{Total}}{d\lambda_s} = 0 = \frac{1}{R_{eq}} [2A_1 A_2 i_{dr}(1+A^2) + 2\lambda_s A_1^2(1+A^2)] + \frac{2\lambda_s R_s}{L_{Ls}^2} - \frac{2R_s L_m}{L_{Ls}^2} i_{dr} = 0$$

$$\lambda_{smin} = \frac{[R_r R_{eq} L_m - (1+A^2)A_1 A_2 L_{Ls}^2] i_{dr}}{A_1^2(1+A^2)L_{Ls}^2 + R_s R_{eq}} \quad (37)$$

The flux at which minimum loss occurred is as presented in (37). This implies that the minimum flux increases with a proportionate rise in the rotor direct axis current and equivalent core resistance values. Therefore, the overall total loss is minimized when  $\lambda_{smin}$  is substituted for  $\lambda_s$  in (36) that gives rise to (38).

$$P_{\text{Loss-min}}^{\text{Total}} = P_{\text{core-min}}^{\text{Total}} + P_{\text{Resistive-min}}^{\text{Total}} + P_{\text{RL-Filter}} + P_{\text{Friction}} + P_{\text{Converter}} = \frac{1}{R_{\text{eq}}} [A_2^2 (1 + A^2) i_r^2 + 2A_1 A_2 \lambda_{\text{smin}} i_{\text{dr}} (1 + A^2) + A_1^2 \lambda_{\text{smin}}^2 (1 + A^2)] + \frac{R_s (\lambda_{\text{smin}})^2}{L_{\text{Ls}}^2} + \frac{R_s L_m^2}{L_{\text{Ls}}^2} i_r^2 - \frac{2R_s L_m}{L_{\text{Ls}}^2} \lambda_{\text{smin}} i_{\text{dr}} + R_r i_r^2 + R_{\text{fe}} [i_{\text{qfe}}^2 + i_{\text{dfe}}^2] + R_{\text{Filter}} (i_{\text{d-Filter}}^2 + i_{\text{q-Filter}}^2) + K_{\text{Fr}} \omega_{\text{mech}}^2 + R_{\text{Converter}} (i_{\text{d-Converter}}^2 + i_{\text{q-Converter}}^2) \quad (38)$$

The DFIG power loss minimization technique applied on (38) was actualized with the Sylvester's criterion for positive definite state using the Hessian matrix determinant test. The objective function to be minimized is the overall total power loss already given in (38). The Hessian matrix is obtained by taking the second derivatives of (38) in terms of stator flux and rotor current as presented (39)–(42).

$$H_{11} = \frac{d^2 P_{\text{Loss-min}}^{\text{Total}}}{d^2 \lambda_{\text{smin}}} = \frac{1}{R_{\text{eq}}} [2(1 + A^2) A_1^2] + \frac{2R_s}{L_s^2} \quad (39)$$

$$H_{12} = \frac{d^2 P_{\text{Loss-min}}^{\text{Total}}}{d\lambda_{\text{smin}} di_r} = 0 \quad (40)$$

$$H_{21} = \frac{d^2 P_{\text{Loss-min}}^{\text{Total}}}{di_r d\lambda_{\text{smin}}} = 0 \quad (41)$$

$$H_{22} = \frac{d^2 P_{\text{Loss-min}}^{\text{Total}}}{d^2 i_r} = \frac{1}{R_{\text{eq}}} [2(1 + A^2) A_2^2] + \frac{2L_m^2 R_s}{L_s^2} + 2R_r \quad (42)$$

The Hessian matrix equation is presented in (43) for the DFIG total loss parameter stability test.

$$H = \begin{bmatrix} H_{11} = \frac{1}{R_{\text{eq}}} [2(1 + A^2) A_1^2] + \frac{2R_s}{L_s^2} & H_{12} = 0 \\ H_{21} = 0 & H_{22} = \frac{1}{R_{\text{eq}}} [2(1 + A^2) A_2^2] + \frac{2L_m^2 R_s}{L_s^2} + 2R_r \end{bmatrix} \quad (43)$$

The total power loss is minimized if the leading principal determinants of (43) are positive and greater than zero. The principal determinants are obtained with the DFIG parameters in Table 2 substituted to give the following:

$$\begin{aligned} |H_{11}| &= \left| \frac{1}{R_{\text{eq}}} [2(1 + A^2) A_1^2] + \frac{2R_s}{L_s^2} \right| = 691.9801 \\ \begin{vmatrix} H_{11} & H_{12} \\ H_{21} & H_{22} \end{vmatrix} &= \begin{vmatrix} \frac{1}{R_{\text{eq}}} [2(1 + A^2) A_1^2] + \frac{2R_s}{L_s^2} & 0 \\ 0 & \frac{1}{R_{\text{eq}}} [2(1 + A^2) A_2^2] + \frac{2L_m^2 R_s}{L_s^2} + 2R_r \end{vmatrix} \\ &= \frac{1}{R_{\text{eq}}^2} \left[ \left( [2(1 + A^2) A_1^2] + \frac{2R_s}{L_s^2} \right) \left( [2(1 + A^2) A_2^2] + \frac{2L_m^2 R_s}{L_s^2} + 2R_r \right) - 0 \right] \\ &= 2.9156e + 05 \end{aligned}$$

The parameters substituted above showed that the DFIG power loss model was controllable with a positive definite value of 691.9801 and  $2.9156 \times 10^5$  for the leading principal determinants of the Hessian matrix. For dynamic simulation analysis of the doubly fed induction generator under a load disturbance, the state space model equations were derived with the aid of Figures 5 and 6 and presented in (44)–(57). Applying the Kirchhoff's current law at nodes A and B on the simplified DFIG dq-axes equivalent circuit diagram presented in Figures 5 and 6 gives rise to (44)–(47).

$$i_{\text{ds}} + i_{\text{dr}} = i_{\text{dfe}} + i_{\text{dm}} \quad (44)$$

$$i_{\text{qs}} + i_{\text{qr}} = i_{\text{qfe}} + i_{\text{qm}} \quad (45)$$

$$i_{\text{dfe}} = i_{\text{ds}} + i_{\text{dr}} - i_{\text{dm}} \quad (46)$$

$$i_{qfe} = i_{qs} + i_{qr} - i_{qm} \quad (47)$$

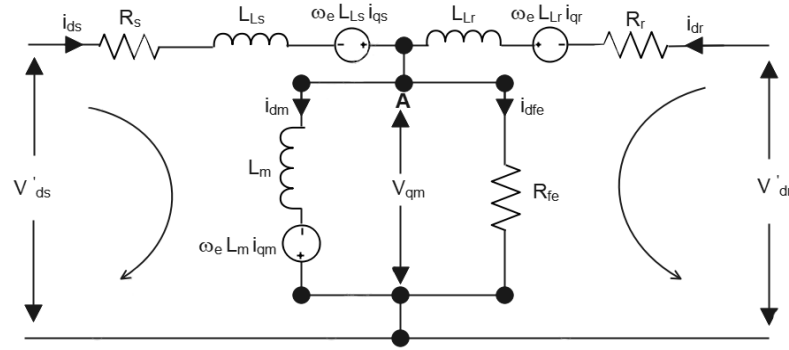


Figure 5. D-axis equivalent circuit of a DFIG with single core resistance

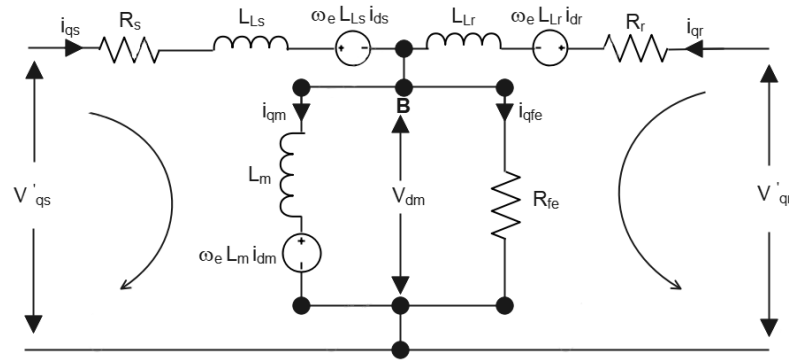


Figure 6. Q-axis equivalent circuit of a DFIG with single core resistance

Sets of current differential equations applied in the DFIG simulations are presented in (48) to (53).

$$\frac{di_{ds}}{dt} = \frac{1}{L_{Ls}} (V_{ds} - R_s i_{ds} + \omega_e L_{Ls} i_{qs} - R_{fe} i_{dfe}) \quad (48)$$

$$\frac{di_{qs}}{dt} = \frac{1}{L_{Ls}} (V_{qs} - R_s i_{qs} - \omega_e L_{Ls} i_{ds} - R_{fe} i_{qfe}) \quad (49)$$

$$\frac{di_{dr}}{dt} = \frac{1}{L_{Lr}} (V_{dr} - R_r i_{dr} - \omega_e L_m i_{qm} + \omega_e L_{Lr} i_{qr} - R_{fe} i_{dfe}) \quad (50)$$

$$\frac{di_{qr}}{dt} = \frac{1}{L_{Lr}} (V_{qr} - R_r i_{qr} - \omega_e L_m i_{dm} + \omega_e L_{Lr} i_{dr} - R_{fe} i_{qfe}) \quad (51)$$

$$\frac{di_{dm}}{dt} = \frac{1}{L_m} (R_{fe} i_{dfe} + \omega_e L_m i_{qm}) \quad (52)$$

$$\frac{di_{qm}}{dt} = \frac{1}{L_m} (R_{fe} i_{qfe} - \omega_e L_m i_{dm}) \quad (53)$$

Similarly, derivatives of (46) and (47) for a change in the core current gave rise to (54) and (55).

$$\frac{di_{dfe}}{dt} = \frac{di_{ds}}{dt} + \frac{di_{dr}}{dt} - \frac{di_{dm}}{dt} \quad (54)$$

$$\frac{di_{qfe}}{dt} = \frac{di_{qs}}{dt} + \frac{di_{qr}}{dt} - \frac{di_{qm}}{dt} \quad (55)$$



The estimated stator active and reactive powers are expressed in (56).

$$\begin{aligned} P_s &= \frac{3}{2} [V_{ds} i_{ds} + V_{qs} i_{qs}] \\ Q_s &= \frac{3}{2} [V_{qs} i_{ds} - V_{ds} i_{qs}] \end{aligned} \quad (56)$$

Also, the estimated rotor active and reactive powers are expressed in (57).

$$\begin{aligned} P_r &= \frac{3}{2} [V_{dr} i_{dr} + V_{qr} i_{qr}] \\ Q_r &= \frac{3}{2} [V_{qr} i_{dr} - V_{dr} i_{qr}] \end{aligned} \quad (57)$$

The mechanical dynamics of the DFIG based on speed and torque are presented in (58)–(60).

$$T_{em} = \frac{3}{2} \times L_m (i_{dm} i_{qr} - i_{qm} i_{dr}) \quad (58)$$

$$\frac{d\omega_r}{dt} = \frac{1}{J} \times (T_e - T_L - \beta \omega_r) \quad (59)$$

$$\omega_r = \int \frac{1}{J} \times (T_e - T_L - \beta \omega_r) \quad (60)$$

The efficiency of the machine in terms of power output and total losses of the DFIG is expressed in (61).

$$\eta = \frac{\text{Power Output}}{\text{Power Output} + \text{Total Losses}} = \frac{T_{em} \times \omega_r}{(T_{em} \times \omega_r) + P_{\text{Total Loss}}} \times 100\% \quad (61)$$

## 5. RESULTS AND DISCUSSION

The simulation parameters are presented in Tables 1 and 2. A plot of the derived flux linkage against the d-axis rotor current at varying core resistance is shown in Figure 7(a). It is observed that the flux linkage increases in linear proportion with the d-axis current with a corresponding rise in the slope and attains a higher value with a reduced equivalent core-resistance ( $R_{eq} = \frac{R_{fe}}{10}$ ). In Figure 7(b) an exponential rise in the total core loss was observed. The deviation in the exponential curve with higher value of core loss (900 kW) is more pronounced when  $R_{eq} = \frac{R_{fe}}{10}$  which implies that more field current and circulating flux is produced at a lower core-resistance. In Figure 8(a), a plot of the total resistive loss against current was presented at a varying rotor resistance. It is also observed that as the resistance value is increased to  $R_r = 40 \times 2.25\Omega$ , the total resistive loss obtained peaked at 2000kW at a current value of 3.25A as against 3.5A got when the rotor resistance was reduced which accounted for the higher current flow through the path of least resistance. In Figure 8(b), it is observed that the DFIG total power loss rose to a value of 3250 kW at a reduced core resistance value of  $R_{eq} = \frac{R_{fe}}{10}$  and higher rotor resistance value of  $R_r = 40 \times 2.25\Omega$  with a rise in slope. This indicates that at reduced core resistance, more field current is drawn since more paralleled resistance is needed to achieve this process whereas with an increased rotor resistance, more power is dissipated across the rotor terminal. The dq-axes voltages for the grid side converter (GSC) and rotor side converter (RSC) are presented in Figures 9(a) and 9(b). It is observed that the voltage magnitude is maintained at 450V during the simulation period thereby ensuring system stability in supply. In Figures 10(a) and 10(b), dq-axes rotor currents are shown at variable core resistance values of  $R_{fe} = 0.75\Omega$  and  $0.25\Omega$ . Similarly, in Figures 11(a) and 11(b), the plots obtained for the dq-axes core current showed that transient disturbance has more impacts on the DFIG core winding at a reduced core resistance value of  $R_{fe} = 0.25\Omega$  and this accounted for its low efficiency value. In Figures 12(a) and 12(b), a sharp deviation in the settling time of the dq-axes magnetizing currents were observed at different core resistance values. The plots for the motor speed and electromechanical torques for different core resistance values are shown in Figures 13(a) and 13(b). It is observed that the transient response in speed and torque is reduced during the period of transient disturbance for  $R_{fe} = 0.75\Omega$  but more oscillatory transient response was obtained after the disturbance was cleared. The power losses and power outputs obtained during a transient disturbance at core resistance values of  $R_{fe} = 0.75\Omega$  and  $0.25\Omega$  are shown in Figures 14(a) and 14(b). It is shown that more losses were obtained in Figure 14(b) with a value of 757.325 kW than in Figure 14(a) that dissipated 202.274 kW. This accounted for the large variation in their efficiency value of 83.45% and 41.21%.

In Figures 15(a) and 15(b), the stator active and reactive powers are presented. It is observed that a rapid oscillation was obtained during a transient disturbance which is more pronounced when the core resistance is kept at  $R_{fe} = 0.75\Omega$ . Conversely, in Figures 16(a) and 16(b), during a transient disturbance a rapid transient oscillation was observed at  $R_{fe} = 0.25\Omega$  for rotor active and reactive power which implies that more current is drawn when  $R_{fe} = 0.25\Omega$ .

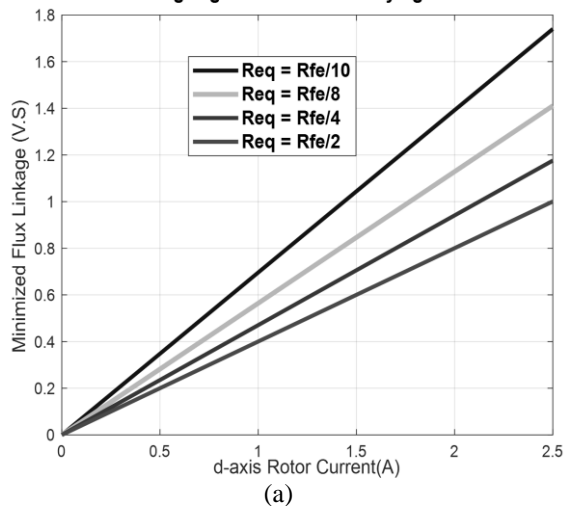
Table 1. Simulation parameters of the turbine blade model

Parameters	Values
Blade radius (m)	1
Maximum power coefficient (Cp)	0.5
Optimal tip speed ratio	10
Cut in speed (m/s)	4.5
Rated wind speed (m/s)	13.5
Minimum Pitch angle (degree)	0
Maximum Pitch angle (degree)	30

Table 2. Simulation parameters used for the DFIG dynamic model

Parameters	Values
Rated power (MW)	15
Rated mechanical power (MW)	10
Supply Voltage (V)	400
Supply Frequency (Hz)	50
Stator resistance (pu)	0.25
Rotor resistance (pu)	0.45
Stator leakage inductance (pu)	0.0877
Rotor leakage inductance (pu)	0.077
Mutual inductance (pu)	0.955
Core resistance of modified circuit ( $\Omega$ )	2.25
Core resistance of simplified circuit (pu)	0.25 and 0.75
Filter resistance (pu)	0.03
Filter inductance (pu)	0.25
Converter resistance (pu)	0.001
Motor inertia Kg-M <sup>2</sup> )	0.045
Coefficient of Viscosity (NMS)	0.00006
Pole pair	2
Load torque (NM)	20

A Plot of Flux Linkage against Current at varying Core Resistance



A Plot of DFIG Core Loss against minimized Flux linkage (V.S)

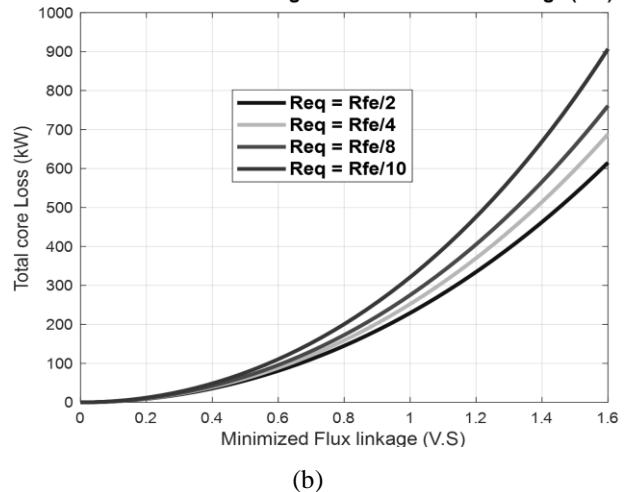


Figure 7. A plot of (a) flux linkage (V.S) against current (A) and (b) total core loss (W) against flux linkage (V.S)

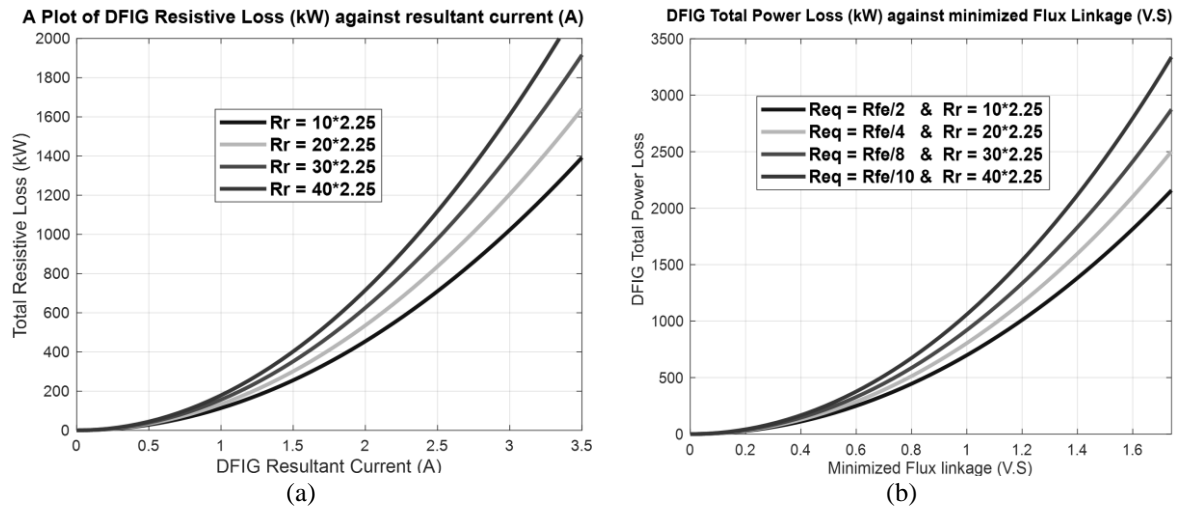


Figure 8. A plot of (a) total resistive loss (W) against current (A) and (b) DFIG total loss (W) against flux linkage (V.S)

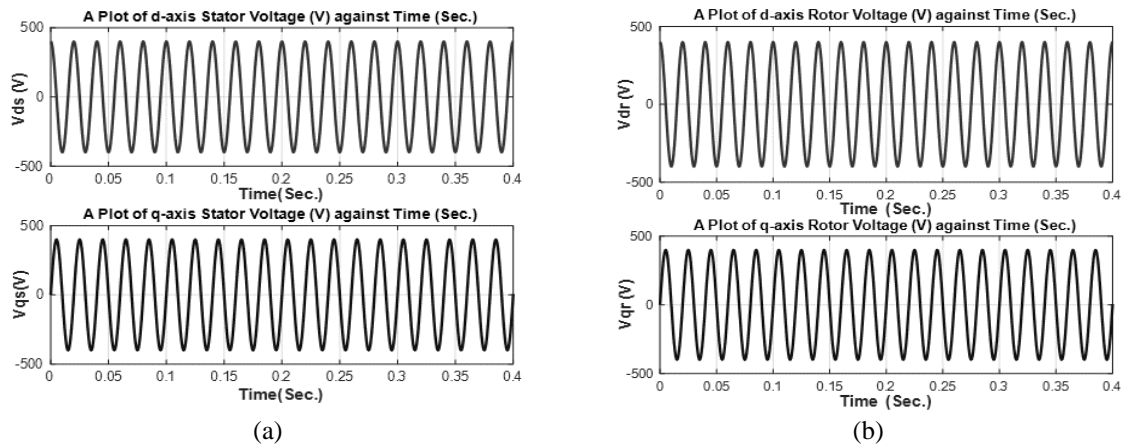


Figure 9. A plot of (a) dq-axes GSC voltage (V) against time (S) and (b) dq-axes RSC voltage (V) against time (S)

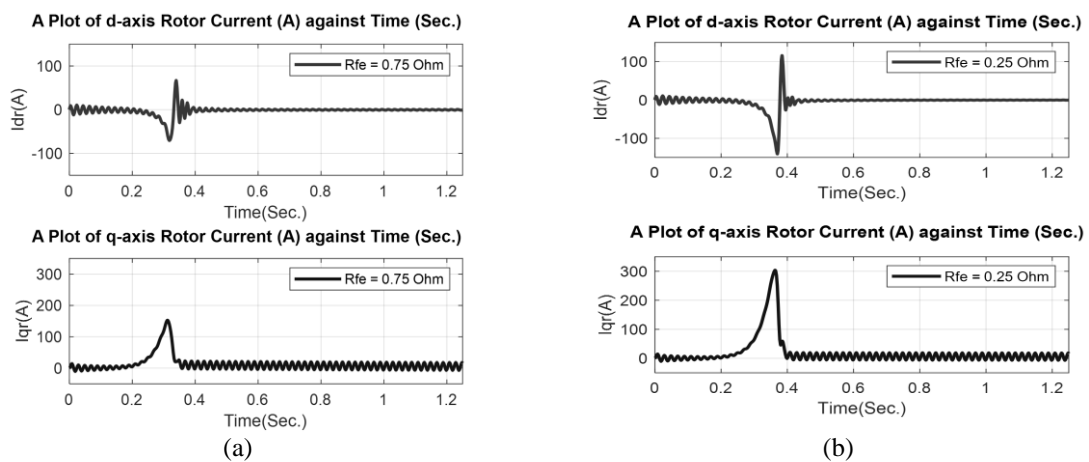


Figure 10. A plot of (a) dq-axes rotor current (A) for  $R_{fe} = 0.75 \Omega$  and (b) dq-axes rotor current for  $R_{fe} = 0.25 \Omega$

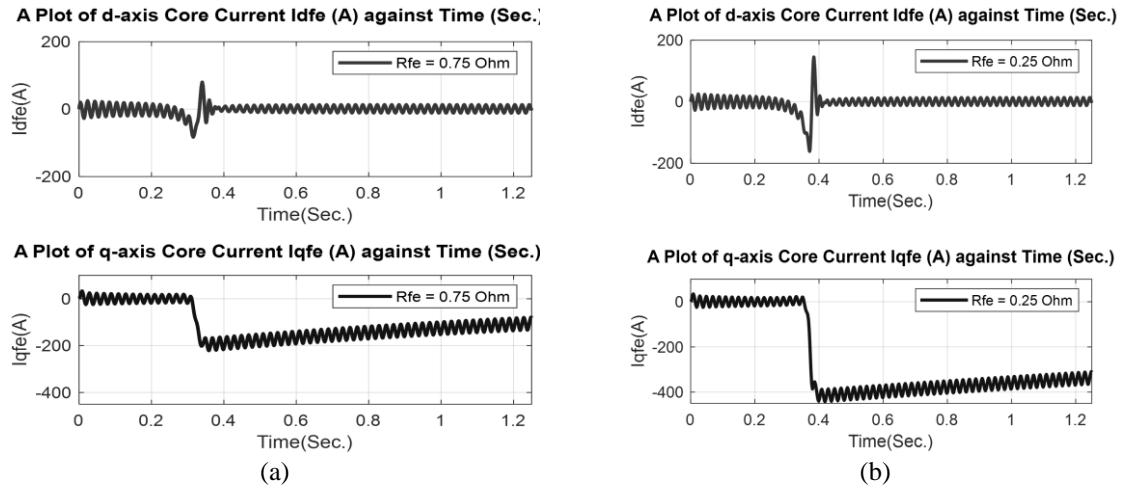


Figure 11. The plots obtained for (a) dq-axes core current (A) for  $R_{fe} = 0.75 \Omega$ . and (b) dq-axes core currents for  $R_{fe} = 0.25 \Omega$

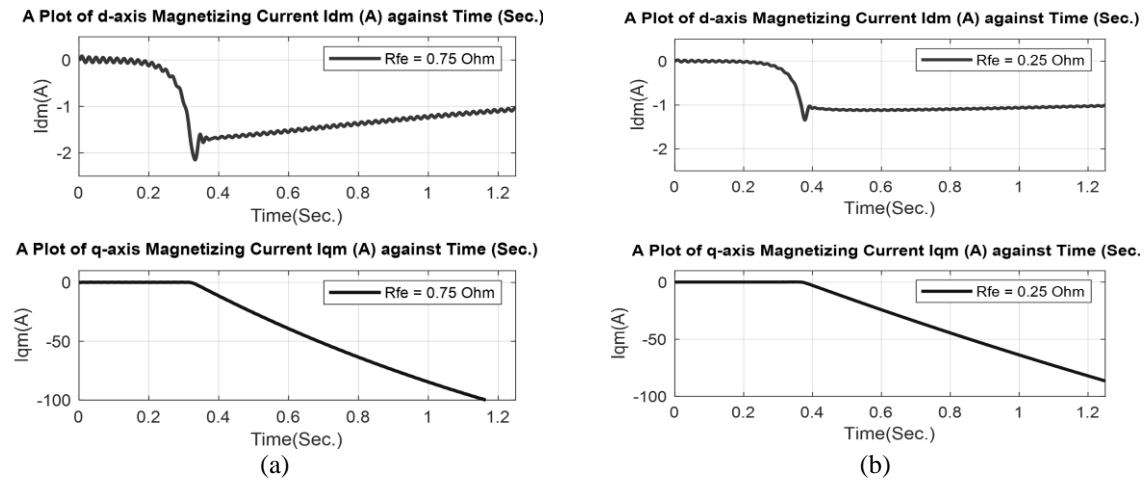


Figure 12. A sharp deviation in the settling time of (a) dq-axes magnetizing current (A) for  $R_{fe} = 0.75 \Omega$  and (b) dq-axes magnetizing currents for  $R_{fe} = 0.25 \Omega$

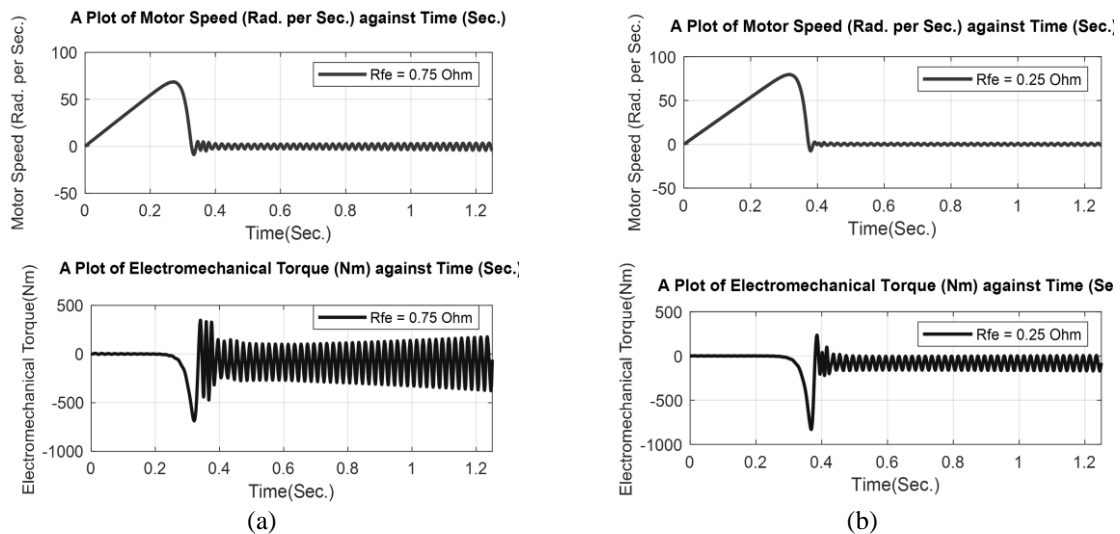


Figure 13. A plot of (a) speed (Rad/Sec) and torque (Nm) for  $R_{fe} = 0.75 \Omega$  and (b) for  $R_{fe} = 0.25 \Omega$

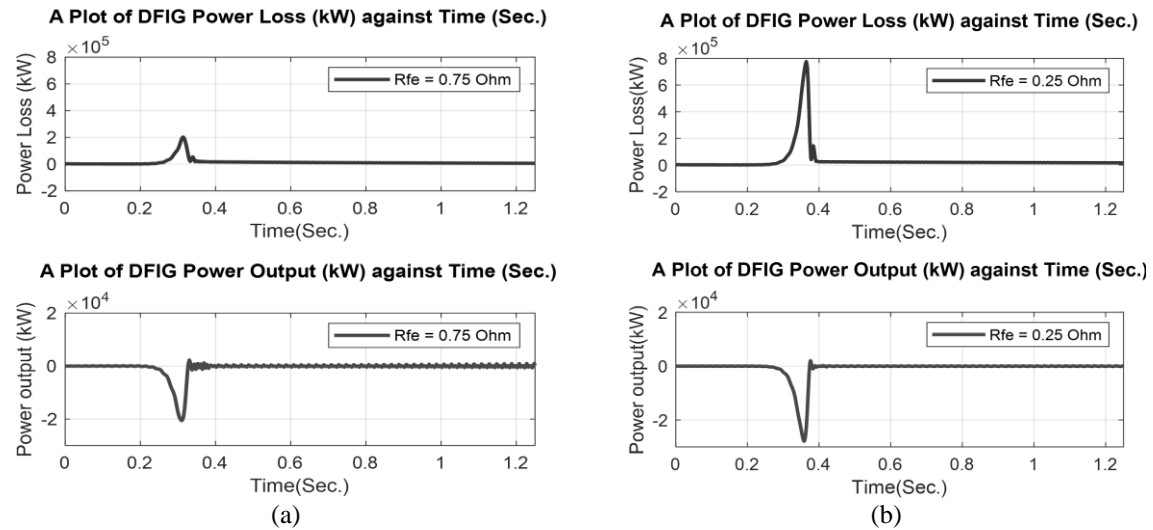


Figure 14. A plot of power loss and power output (kW) for (a)  $R_{fe}=0.75\Omega$  and (b)  $R_{fe} = 0.25\Omega$

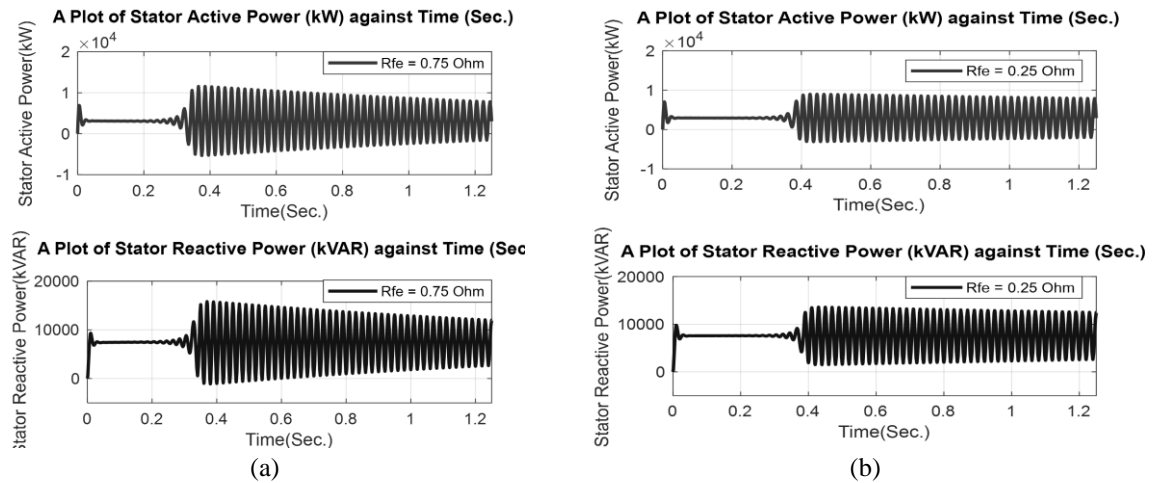


Figure 15. A plot of stator active and reactive power for (a)  $R_{fe} = 0.75\Omega$  and (b)  $R_{fe} = 0.25\Omega$

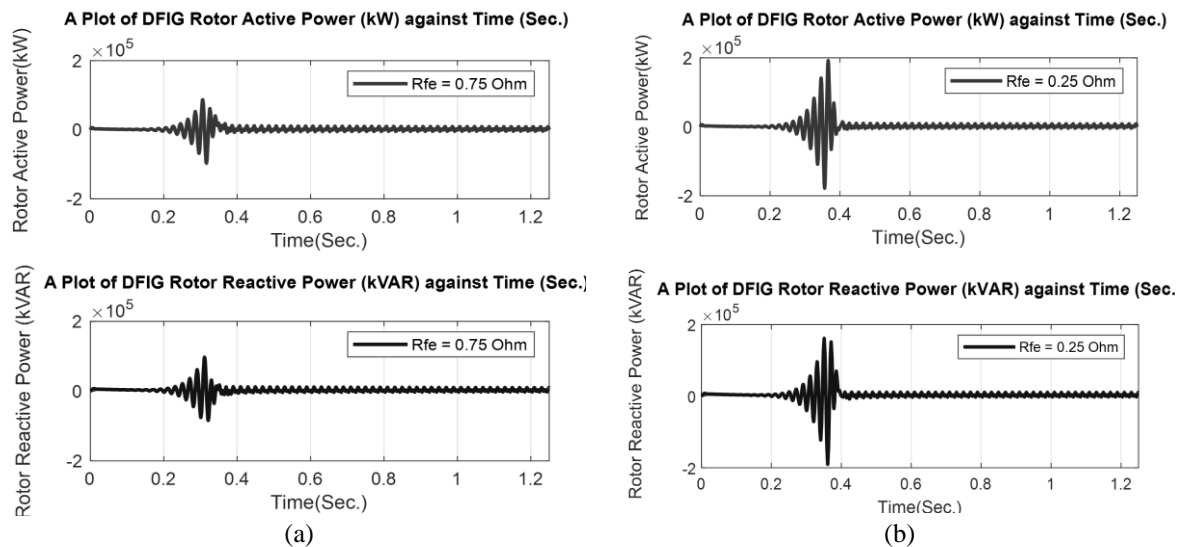


Figure 16. A plot of rotor active and reactive power for (a)  $R_{fe} = 0.75\Omega$ . and (b)  $R_{fe} = 0.25\Omega$

## 6. CONCLUSION

In this paper, power loss minimization of a DFIG has been presented using a modified DFIG equivalent circuit with multi-core resistances connected in parallel. The impact of core arrangements on dynamic power loss inside a DFIG was analyzed. The loss minimization model of the DFIG was developed incorporating iron, copper loss components, RL-filter losses, Frictional losses and power electronics converter losses with a minimum flux linkage to minimize the overall total power losses. Simulation results showed that losses are minimized when the equivalent core resistances are connected in parallel with minimum permissible current flow. This aids in regulating the magnitude of the reactive power between the wind turbine and the DFIG. An unconstrained optimization carried out showed that the DFIG power loss model analyzed using the Hessian matrix is positive definite and therefore is controllable. The results obtained during a transient disturbance indicated that at different core resistance values of  $R_{fe} = 0.75\Omega$  and  $0.25\Omega$  different efficiency values of 83.45% and 41.20% were obtained due to the variation in the core currents and core losses. It can be concluded from the simulation results that with the reduced core resistance and increased flux linkage more current flows through the core and more losses are dissipated with a consequent local saturation of the core which may be unavoidable.




## REFERENCES

- [1] M. Edrah, K. L. Lo, and O. Anaya-Lara, "Impacts of high penetration of DFIG wind turbines on rotor angle stability of power systems," *IEEE Trans. Sustain. Energy*, vol. 6, no. 3, pp. 759–766, 2015, doi: 10.1109/TSTE.2015.2412176.
- [2] S. Tohidi and M. I. Behnam, "A comprehensive review of low voltage ride through of doubly fed induction wind generators," *Renew. Sustain. Energy Rev.*, vol. 57, pp. 412–419, 2016, doi: 10.1016/j.rser.2015.12.155.
- [3] V. Yaramasu, B. Wu, P. C. Sen, S. Kouro, and M. Narimani, "High-power wind energy conversion systems: State-of-the-art and emerging technologies," *Proc. IEEE*, vol. 103, no. 5, pp. 740–788, May 2015, doi: 10.1109/JPROC.2014.2378692.
- [4] H. Jabbari Asl and J. Yoon, "Power capture optimization of variable-speed wind turbines using an output feedback controller," *Renew. Energy*, vol. 86, pp. 517–525, 2016, doi: 10.1016/j.renene.2015.08.040.
- [5] T. Dinesh and R. Rajasekaran, "Independent operation of DFIG-based WECS using resonant feedback compensators under unbalanced grid voltage conditions," in *2015 International Conference on Innovations in Information, Embedded and Communication Systems (ICIIECS)*, Mar. 2015, vol. 30, no. 7, pp. 1–8, doi: 10.1109/ICIIECS.2015.7192996.
- [6] F. M. Ebrahimi, A. Khayatiyan, and E. Farjah, "A novel optimizing power control strategy for centralized wind farm control system," *Renew. Energy*, vol. 86, pp. 399–408, 2016, doi: 10.1016/j.renene.2015.07.101.
- [7] M. H. Baloch, J. Wang, and G. S. Kaloi, "Stability and nonlinear controller analysis of wind energy conversion system with random wind speed," *Int. J. Electr. Power Energy Syst.*, vol. 79, pp. 75–83, 2016, doi: 10.1016/j.ijepes.2016.01.018.
- [8] H. Nian, P. Cheng, and Z. Q. Zhu, "Coordinated direct power control of dfig system without phase-locked loop under unbalanced grid voltage conditions," *IEEE Trans. Power Electron.*, vol. 31, no. 4, pp. 2905–2918, 2016, doi: 10.1109/TPEL.2015.2453127.
- [9] M. K. Bourdoulis and A. T. Alexandridis, "Direct power control of DFIG wind systems based on nonlinear modeling and analysis," *IEEE J. Emerg. Sel. Top. Power Electron.*, vol. 2, no. 4, pp. 764–775, 2014, doi: 10.1109/JESTPE.2014.2345092.
- [10] P. Xiong and D. Sun, "Backstepping-Based DPC Strategy of a Wind Turbine-Driven DFIG Under Normal and Harmonic Grid Voltage," *IEEE Trans. Power Electron.*, vol. 31, no. 6, pp. 4216–4225, Jun. 2016, doi: 10.1109/TPEL.2015.2477442.
- [11] X. Wang, D. Sun, and Z. Q. Zhu, "Resonant-Based Backstepping Direct Power Control Strategy for DFIG under Both Balanced and Unbalanced Grid Conditions," *IEEE Trans. Ind. Appl.*, vol. 53, no. 5, pp. 4821–4830, 2017, doi: 10.1109/TIA.2017.2700280.
- [12] M. El Azzouli, H. Mahmoudi, and C. Ed-Dahmani, "Backstepping control of a Doubly Fed Induction Generator integrated to wind power system," *Proc. 2016 Int. Conf. Electr. Inf. Technol. ICEIT 2016*, pp. 306–311, 2016, doi: 10.1109/EITech.2016.7519611.
- [13] B. Bossoufi, M. Karim, A. Lagrioui, M. Taoussi, and A. Derouich, "Observer backstepping control of DFIG-Generators for wind turbines variable-speed: FPGA-based implementation," *Renew. Energy*, vol. 81, pp. 903–917, Sep. 2015, doi: 10.1016/j.renene.2015.04.013.
- [14] J. Koupeny, M. Siebrecht, S. Lücke, and A. Mertens, "Observer-based online parameter estimation of doubly fed induction generators based on the gradient descent method," *Int. ETG Congr. 2015; Die Energiewende - Blueprints New Energy Age*, 2015.
- [15] Y. T. Weng and Y. Y. Hsu, "Sliding mode regulator for maximum power tracking and copper loss minimisation of a doubly fed induction generator," *IET Renew. Power Gener.*, vol. 9, no. 4, pp. 297–305, 2015, doi: 10.1049/iet-rpg.2014.0125.
- [16] I. K. Amin and M. N. Uddin, "Nonlinear control operation of DFIG based WECS with stability analysis," *2017 IEEE Ind. Appl. Soc. Annu. Meet. IAS 2017*, vol. 2017-January, pp. 1–8, 2017, doi: 10.1109/IAS.2017.8101789.
- [17] P. Kou, D. Liang, F. Gao, and L. Gao, "Coordinated Predictive Control of DFIG-Based Wind-Battery Hybrid Systems: Using Non-Gaussian Wind Power Predictive Distributions," *IEEE Trans. Energy Convers.*, vol. 30, no. 2, pp. 681–695, 2015, doi: 10.1109/TEC.2015.2390912.
- [18] A. Yousefi-Talouki, E. Pouresmaeil, and B. N. Jørgensen, "Active and reactive power ripple minimization in direct power control of matrix converter-fed DFIG," *Int. J. Electr. Power Energy Syst.*, vol. 63, pp. 600–608, 2014, doi: 10.1016/j.ijepes.2014.06.041.
- [19] P. K. Gayen, D. Chatterjee, and S. K. Goswami, "Stator side active and reactive power control with improved rotor position and speed estimator of a grid connected DFIG (doubly-fed induction generator)," *Energy*, vol. 89, pp. 461–472, 2015, doi: 10.1016/j.energy.2015.05.111.
- [20] K. E. Okedu, "Augmentation of DFIG and PMSG Wind Turbines Transient Performance Using Different Fault Current Limiters," *Energies*, vol. 15, no. 13, 2022, doi: 10.3390/en15134817.
- [21] K. E. Okedu, "Enhancing the performance of DFIG variable speed wind turbine using a parallel integrated capacitor and modified modulated braking resistor," *IET Gener. Transm. Distrib.*, vol. 13, no. 15, pp. 3378–3387, 2019, doi: 10.1049/iet-gtd.2019.0206.
- [22] K. E. Okedu, "Improving the transient performance of DFIG wind turbine using pitch angle controller low pass filter timing and network side connected damper circuitry," *IET Renew. Power Gener.*, vol. 14, no. 7, pp. 1219–1227, 2020, doi: 10.1049/iet-rpg.2019.1124.




- [23] A. Parida and D. Chatterjee, "Model-based loss minimisation scheme for wind solar hybrid generation system using (grid-connected) doubly fed induction generator," *IET Electr. Power Appl.*, vol. 10, no. 6, pp. 548–559, 2016, doi: 10.1049/iet-epa.2016.0040.
- [24] G. S. Kaloi, J. Wang, and M. H. Baloch, "Active and reactive power control of the doubly fed induction generator based on wind energy conversion system," *Energy Reports*, vol. 2, pp. 194–200, 2016, doi: 10.1016/j.egy.2016.08.001.

## BIOGRAPHIES OF AUTHORS



**Crescent Onyebuchi Omeje**    is a Senior Lecturer in the Department of Electrical Electronic Engineering, University of Port Harcourt, Port Harcourt River State Nigeria. He graduated from the University of Nigeria, Nsukka in the Department of Electrical Engineering. He has published widely in local and international journals. His research work focuses on power electronics, new energy conversion system, multilevel inverter applications, Electric motor drives and Power systems modeling and simulation. He is a member of the Institute of Electrical/Electronic Engineering (IEEE), a member of the Nigerian Society of Engineers (NSE) and he is also a registered member of the Council for the Regulation of Engineering in Nigeria (COREN). He can be contacted at email: [crescent.omeje@uniport.edu.ng](mailto:crescent.omeje@uniport.edu.ng).



**Damian Benneth Nnadi**    is presently a Professor in the Department of Electrical Engineering UNN. His university education was at Enugu State University of Science and Technology (ESUT), Enugu from 1993 to 1999, there, he obtained a B.Eng. (Electrical/Electronic). He got his M.Eng. degree also from Enugu State University of Science and Technology (ESUT) from 2002 to 2004. He has also obtained a Ph. D. in Power Electronics option from Electrical Engineering, University of Nigeria, Nsukka in 2014. He is a member of the Nigerian Society of Engineers (NSE). He is the current financial secretary of Nsukka Chapter of the Nigerian Institute of Electrical and Electronic Engineering (NIEEE) and he is also a registered member of the Council for the Regulation of Engineering in Nigeria (COREN). He is a member of the Industrial/Power Electronics and New/Renewable Energy Research Group, Power system/High Voltage Research Group. He can be contacted at email: [damian.nnadi@unn.edu.ng](mailto:damian.nnadi@unn.edu.ng).